Temporal and Spatial Variability of Wind Resources in the United States as Derived from the Climate Forecast System Reanalysis

LEJIANG YU

Applied Hydrometeorological Research Institute, Nanjing University of Information Science and Technology, Nanjing, China, and Department of Geography, and Center for Global Change and Earth Observations, Michigan State University, East Lansing, Michigan

SHIYUAN ZHONG

Department of Geography, and Center for Global Change and Earth Observations, Michigan State University, East Lansing, Michigan

XINDI BIAN AND WARREN E. HEILMAN

Northern Research Station, USDA Forest Service, Lansing, Michigan

(Manuscript received 30 April 2014, in final form 27 October 2014)

ABSTRACT

This study examines the spatial and temporal variability of wind speed at 80 m above ground (the average hub height of most modern wind turbines) in the contiguous United States using Climate Forecast System Reanalysis (CFSR) data from 1979 to 2011. The mean 80-m wind exhibits strong seasonality and large spatial variability, with higher (lower) wind speeds in the winter (summer), and higher (lower) speeds over much of the Midwest and U.S. Northeast (U.S. West and Southeast). Trends are also variable spatially, with more upward trends in areas of the Great Plains and Intermountain West of the United States and more downward trends elsewhere. The leading EOF mode, which accounts for 20% (summer) to 33% (winter) of the total variance and represents in-phase variations across the United States, responds mainly to the North Atlantic Oscillation (NAO) in summer and El Niño–Southern Oscillation (ENSO) in the other seasons. The dominant variation pattern can be explained by a southerly/southwesterly (westerly) anomaly over the U.S. East (U.S. West) as a result of the anomalous mean sea level pressure (MSLP) pattern. The second EOF mode, which explains about 15% of the total variance and shows a seesaw pattern, is mainly related to the springtime Arctic Oscillation (AO), the summertime recurrent circumglobal teleconnection (CGT), the autumn Pacific decadal oscillation (PDO), and the winter El Niño Modoki. The anomalous jet stream and MSLP patterns associated with these indices are responsible for the wind variation.

1. Introduction

Wind energy has received considerable attention in the United States over the last decade with cumulative wind capacity (the product of total number of wind turbines and rated power) increasing dramatically from 2472 MW in 1999 to 60 009 MW in 2012 (AWEA 2013). The increasing interest in wind energy has promoted numerous investigations into low-level wind climatology and wind power potentials across the United States. Elliott et al. (1986) produced wind energy resource atlases for different regions of the United States. Klink (1999a) examined the climatology and annual cycles of monthly mean wind speed and direction from 1961 to 1990 at 216 surface stations in the contiguous United States. Archer and Jacobson (2003) studied spatial and temporal distributions of winds at 80 m above ground level (AGL) in the United States using data from 1327 surface stations and 87 sounding sites in the year 2000. In an effort to identify an ideal location for a wind energy grid, Kempton et al. (2010) and Dvorak et al. (2012) investigated U.S. East Coast offshore wind energy resources using wind data from a combination of 11

Corresponding author address: Dr. Shiyuan "Sharon" Zhong, Department of Geography, Michigan State University, 673 Auditorium Rd., East Lansing, MI 48824.
E-mail: zhongs@msu.edu

DOI: 10.1175/JCLI-D-14-00322.1

© 2015 American Meteorological Society

meteorological stations and a mesoscale numerical weather prediction model. Li et al. (2010) investigated the wind power resources in the Great Lakes region using the gridded North American Regional Reanalysis (NARR) dataset.

Several previous studies have investigated trends in low-level wind speed in the United States. By examining mean monthly surface wind speed maxima at 187 stations and minima at 176 stations across the conterminous United States, Klink (1999b) found that on balance there was an increasing (decreasing) trend in the mean monthly maximum (minimum) winds from 1961 to 1990. The study attributed these trends to various factors including temperature trends, changes in cyclone and anticyclone frequency, effects of urbanization, and bias in the observations. In another more localized study, Klink (2002) revealed a decreasing trend in the mean annual wind speeds from the 1960s to the 1990s at seven surface stations in and surrounding Minnesota. Similar downward trends of near-surface wind have also been found across the conterminous United States by Pryor et al. (2009), Pryor and Ledolter (2010), and Vautard et al. (2010) based on analyses of data from the National Climatic Data Center from 1973 to 2004. A decline in surface wind speeds has also been observed in other midlatitude regions (Smits et al. 2005; Xu et al. 2006; McVicar et al. 2010; Wan et al. 2010). A summary of various factors that might have contributed to the declining trend of surface wind speeds is given by Vautard et al. (2010). These factors include widening of the Hadley cell and the tropical belt (Lu et al. 2007; Seidel et al. 2008), increases in surface roughness (Smits et al. 2005; McVicar et al. 2010; Pryor et al. 2009), instrumental drift (DeGaetano 1998), and the change in monsoon circulation induced by air pollution (Xu et al. 2006; Hua et al. 2010).

Recently, much attention has been given to the impact of climate change on low-level wind speed and wind energy resource in the United States. Based on the simulations of the Hadley Centre Coupled Model, version 2 (HadCM2), Segal et al. (2001) found that global climate change resulting from an enhanced CO_2 emission may cause a 0%–30% decrease in daily average wind power availability in most regions of the United States. Combining the results from HadCM2 and the CCCma Coupled Global Climate Model (CGCM), Breslow and Sailor (2002) showed that a decrease in wind speed by 1.0%–3.2% and by 1.4%–4.5% may occur in the United States over the next 50 and 100 years, respectively. Sailor et al. (2008) revealed that for the relatively high greenhouse gas emissions scenario [the Special Report on Emission Scenarios (SRES) A2 scenario; Nakicenovic 2000], the summertime wind speeds in the northwestern United States may be decreased by 5%–10% with a 40% reduction in wind power, whereas there would be little decrease or even a slight increase in wintertime wind speeds. Pryor and Barthelmie (2011), however, revealed no clear tendency in the wind energy resource over the contiguous United States over the next 50 years based on the projections from multiple regional climate models.

Although many studies have revealed the climatological characteristics of low-level winds and the projected climate impact on wind resources in the United States, few have focused on the spatial and temporal variability and the cause for the variability. While the diurnal and day-to-day wind variability may be related to changes in stability and weather patterns, the cause for interannual variability is less clear. Understanding the low-frequency variability of wind speeds, or how and why wind speeds and wind power vary from one year to another, can be beneficial for seasonal outlook or long-range forecasting of wind power generation (Westrick et al. 2005).

A number of studies have examined the interannual variability of low-level wind speeds in different regions of the United States and Canada, and they have linked the variability to El Niño–Southern Oscillation (ENSO) climate forcing. Li et al. (2010) studied the interannual variability of the 80-m level winds over the Great Lakes region using the NARR data and found lower mean wind speeds and more frequent occurrences of lulls across the region during El Niño years compared to La Niña years. Using hourly wind speed data from four airport anemometers, Harper et al. (2007) found a significant link between El Niño years and a decreasing mean wind speed and wind power production in the northern plains. St. George and Wolfe (2009) analyzed monthly surface wind observations in the southern Canadian prairies and western Canada and found that nearly all low wind events in the past 50 years in the southern Canadian prairies occurred during a moderate or stronger El Niño. However, based on the simulation results using the MM5 model, Berg et al. (2013) noted an increase (decrease) in regional-averaged mean wind speeds and wind speed variability over southern California during El Niño (La Niña). Besides ENSO, Klink (2007) linked the variability of wind speeds observed at eleven 70-m wind monitoring sites in Minnesota to the Arctic Oscillation (AO) and the Pacific–North American (PNA) pattern. Rauthe et al. (2004) also showed that the strengthening of the AO under future climate change may increase wind speed and wind power in Minnesota. Clifton and Lundquist (2012) found that strong 80-m westerly winds at the National Wind Technology Center in Colorado are negatively

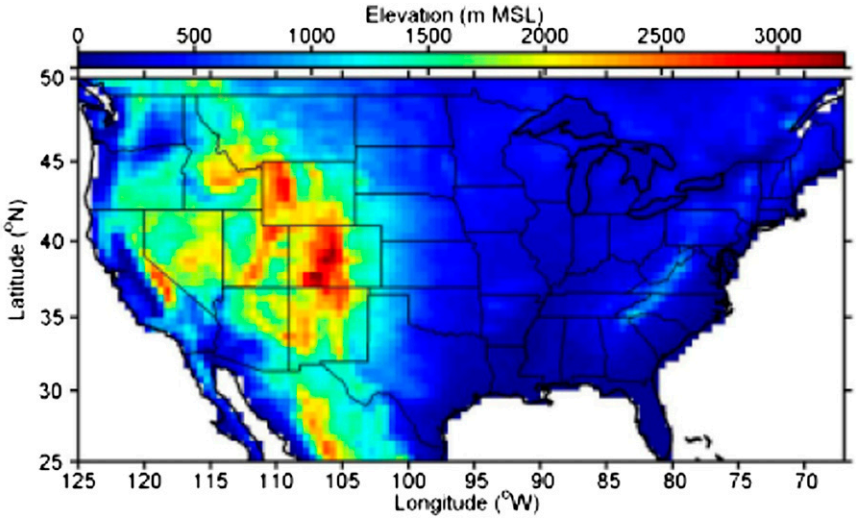

FIG. 1. The study domain (25°–50°N, 125°–67°W) and the topography as resolved in the Climate Forecast System Reanalysis dataset.

correlated with the Niño-3.4 index, while weaker winds appear to be connected to the PNA and AO indices.

The aforementioned studies on low-frequency wind variability have been limited to particular states or specific regions of the United States. Enloe et al. (2004) investigated the relationship between the peak wind gust magnitudes over the contiguous United States and the warm and cold phases of ENSO for the 1948–98 period and found the connection is consistent with the relationship between the precipitation pattern in the United States and ENSO. This study focuses only on peak wind gusts without including mean wind speed or the frequency of different class winds.

The current study investigates the spatial and temporal variability of the modern wind turbine level (80 m above ground level) wind speed climatology in the contiguous United States for a 33-yr period from 1979 through 2011 using a third-generation high-resolution global reanalysis data product. In addition to climatology, the study also identifies and characterizes the main modes of wind speed variability in the contiguous United States and the dominant climate forcing through the use of empirical orthogonal function (EOF) analyses and regression techniques.

2. Datasets and methods

The current study examines wind speeds at the 80-m AGL over the region between 25°–50°N and 125°–67°W, which covers the contiguous United States and parts of southern Canada and northern Mexico (Fig. 1). The study utilizes data from the Climate Forecast System Reanalysis (CFSR) (Saha et al. 2006, 2010) produced by the National Centers for Environmental Prediction (NCEP). CFSR is a third-generation reanalysis product generated by utilizing a suite of observational and model data and coupled atmosphere–ocean–land–sea ice system (Saha et al. 2010). Compared to the previous reanalysis products, CFSR contains a number of new features, including 6-h guess fields generated from a coupled atmosphere–ocean system, a sea ice model that is interactive with the coupled atmosphere–ocean system, assimilation of satellite radiances, and consideration of variations of carbon dioxide (CO_2), aerosols, and other trace gases and solar activity. The global resolution of CFSR is ~38 km (T382 spectral truncation) with 64 levels from the surface to 0.26 hPa for its atmosphere model and 0.25° at the equator and 0.5° beyond the tropics with 40 levels to a depth of 4737 m for its ocean model, with four soil levels for its land model and three layers for its sea ice model. For details about the CFSR, refer to Saha et al. (2010).

Several studies have compared CFSR atmospheric and oceanic variables to observations and to similar products in previous reanalysis datasets (Wang et al. 2011; Xue et al. 2011; Chelliah et al. 2011; Long et al. 2011). These comparisons have shown that CFSR improves the spatial pattern and interannual variability of precipitation and surface air temperature, but overestimates downward solar radiative flux and latent heat flux (Wang et al. 2011). Of particular relevance to this study is that the CFSR's ocean surface wind has smaller errors compared to the QuikSCAT climatology from September 1999 to October 2009 than the early NCEP global reanalysis (Xue et al. 2011). Liléo and Petrik (2011) noted that CFSR made an average improvement of 16% in correlation coefficient with observed wind

speed from 24 masts in Sweden from 1980 to 2009 compared to the earlier NCEP global reanalysis dataset. A recent study by Bao and Zhang (2013) showed that the horizontal winds from CFSR and the European Centre for Medium-Range Weather Forecasts (ECMWF) Interim Re-Analysis (ERA-Interim; Dee et al. 2011) agree with the winds measured by rawinsonde soundings launched during the Tibetan Plateau Experiment (TIPEX) and have smaller root-mean-square errors compared to the earlier global reanalysis products. Rahim et al. (2013) showed a significant correlation between CFSR and QuikSCAT over the South China Sea. Most recently, Chen et al. (2014) assessed the diurnal cycle of wind fields from the Japanese 55-year Reanalysis Project (JRA-55), ERA-Interim, CFSR, and the Modern-Era Retrospective Analysis for Research and Applications (MERRA) over East Asia using rawinsonde observation data from 22 sites over southern China. They noted that the four reanalysis datasets can represent the mean wind diurnal cycle, but they differ in the amplitude of the diurnal cycle.

The current study utilizes the latest version (version 2) of CFSR (CFSv2) (Saha et al. 2014), which improves surface air temperatures and precipitation over the earlier version (CFSv1) by 37% and 29%, respectively (Yuan et al. 2011). The CFSv2 data are archived four times daily from 1979 through 2011 at 37 pressure levels from 1000 to 100 hPa. The vertical resolution is 25 hPa below 750 hPa, decreasing to 50 hPa above that. The 80-m level wind speed is determined by a vertical linear interpolation of wind speeds that are calculated first using the archived zonal and meridional wind components. The interpolation uses wind at 10 m AGL and the wind at the lowest level above 80 m AGL. At each grid point in the study domain, the height of the pressure level is determined by the archived geopotential height fields and the surface elevation. At each grid point, the 6-hourly data are first averaged to yield a daily mean, which is then averaged to obtain monthly and then seasonal mean wind speeds.

In addition to the CFSv2 reanalysis products, the National Oceanic and Atmospheric Administration (NOAA) Extended Reconstructed Sea Surface Temperature (ERSST) dataset (Smith and Reynolds 2003, 2004) is also used for identifying the pattern of SST over the Pacific Ocean.

The data analysis focuses first on the general climatology of the 80-m winds, including seasonal variation, interannual variability as measured by the interannual standard deviation, and linear trend calculated using least squares regression. The significance of the linear trend is tested at each grid point using a standard Student's t test method. In addition, multiple testing using the Benjamini and Hochberg (1995) method also is carried out to control the false discovery rate (FDR).

After examining the climatology, the EOF technique is used to reveal the dominant patterns of the variability of the seasonal mean wind. The EOF analysis can produce a set of modes that consist of spatial structures (EOFs) and corresponding time series [principal components (PCs)]. For each mode, its EOF and PC are orthogonal to the EOFs and PCs of all other modes. Each mode has a corresponding eigenvalue that describes the variance explained by the mode. More details of the EOF technique can be found in Wilks (2011). In this study the EOF technique is utilized to identify the prevailing spatial patterns of seasonal mean wind speed anomalies for spring [March–May (MAM)], summer [June–August (JJA)], autumn [September–November (SON)], and winter [December–February (DJF)]. The anomalous seasonal mean wind speed can be obtained by the seasonal mean wind speed for each year subtracted by the climatological seasonal mean wind speed over the entire study period.

Finally, to explain how the large-scale circulation patterns are likely to influence the leading EOF patterns, regression analysis is performed, which is described briefly below.

At a given grid point, the anomalous season mean atmospheric or oceanic variable is a vector of n dimension with $n = 32$ for winter and $n = 33$ for the other seasons for the study period of January 1979 through December of 2011. In other words, $\mathbf{Y}(y_1, y_2, \ldots, y_i, \ldots, y_n)$ represents a large-scale circulation variable (e.g., 200-hPa geopotential height or SST). The normalized PC is also a vector of the same n dimension, represented by $\mathbf{X}(x_1, x_2, \ldots, x_i, \ldots, x_n)$. A linear regression between $\mathbf{Y}$ and $\mathbf{X}$ can be constructed using

$$y_i = \alpha + \beta x_i + \varepsilon_i,$$

where α is the intercept, β is the slope, and ε_i is a residual term. A least squares approach is used to minimize the sum of squared residuals. The residuals are tested for temporal independence using autocorrelation function. The regression maps in section 3 show the spatial distribution of the β value at each grid point in the study domain for a given large-scale circulation variable, which indicates the changes in the variable associated with the changes in the PC.

3. Results and discussions

In this section, we first examine the climatology, the interannual standard deviations, and the trends of 80-m wind speeds for the 33-yr period from 1979 through

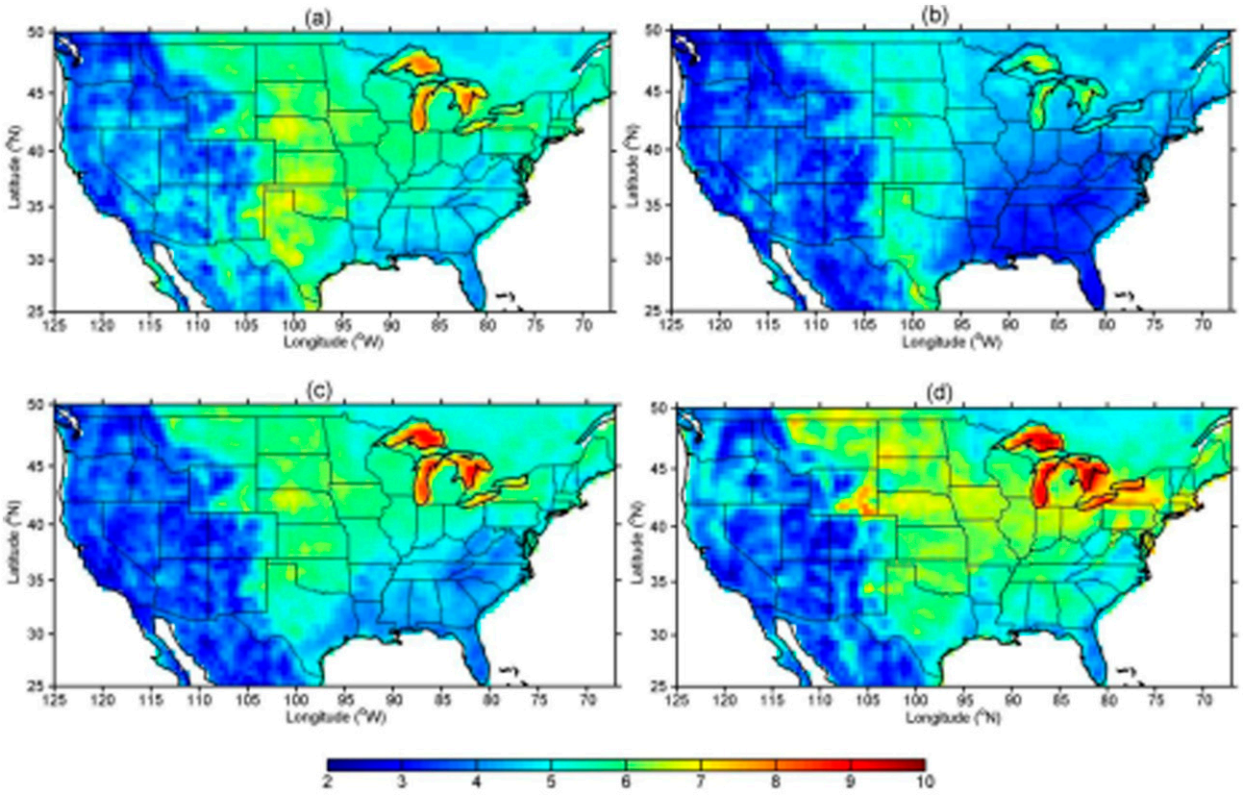

FIG. 2. Climatology of the 80-m wind speed ($m\,s^{-1}$) in (a) spring, (b) summer, (c) autumn, and (d) winter for the period of 1979–2011.

2011. EOF analyses are then performed to reveal the dominant modes of the spatial and temporal variability. Finally, regression analyses are carried out to understand the relationship between the leading EOF modes and large-scale circulation patterns.

a. Climatology of the 80-m winds: Seasonality, interannual variability, and trends

The 80-m wind speed climatology and the seasonal variation obtained by averaging over the 33-yr period for each season are shown in Fig. 2. The climatology exhibits a strong seasonality with the highest seasonal mean wind speeds occurring in the winter and the lowest speeds occurring in the summer. Seasonal mean wind speeds greater than $8\,m\,s^{-1}$ occur mainly over the Great Lakes due to the smaller friction of water surface as compared to land surface. Mean wind speeds higher than $6\,m\,s^{-1}$ are seen over areas of the Great Plains and U.S. Northeast. In the western United States, mean wind speeds are generally less than $5\,m\,s^{-1}$ year round. In summer, wind speeds less than $4\,m\,s^{-1}$ occur in areas of the U.S. Southeast where stagnant conditions occur frequently due to the influence of the Bermuda high (Davis et al. 1997).

At any given location, the seasonal mean 80-m wind speed may vary significantly from year to year, and the standard deviation is used to describe this year-to-year variation (i.e., interannual variability). As shown in Fig. 3, the interannual standard deviations of seasonal mean 80-m wind speeds exhibit a strong seasonality similar to the mean wind speed climatology (Fig. 2). Higher standard deviations are seen in winter while lower deviations are found in summer and autumn. In winter, standard deviations are generally higher over areas of the U.S. Northwest, the Great Plains, and the Northeast, and lower in the U.S. South. In summer, higher values are seen over much of the Midwest. In autumn, standard deviations are higher over much of the Northeast and the Great Lakes region and parts of the Northwest. In spring, they are higher over the Northeast, the southern Great Plains, and the Rockies.

The linear trends in the seasonal mean 80-m wind speed for the 33-yr period are calculated using least squares regression and the results shown in Fig. 4. Significant upward trends occur in areas of the Great Plains, the Intermountain West of the United States, and along parts of the Gulf coast from Louisiana through Alabama, while significant downward trends occur over areas of the Midwest, the Northeast, the Southeast, and areas of the Pacific coast. In winter, significant upward trends occur only in areas of the U.S. Southwest and southeastern Canada and

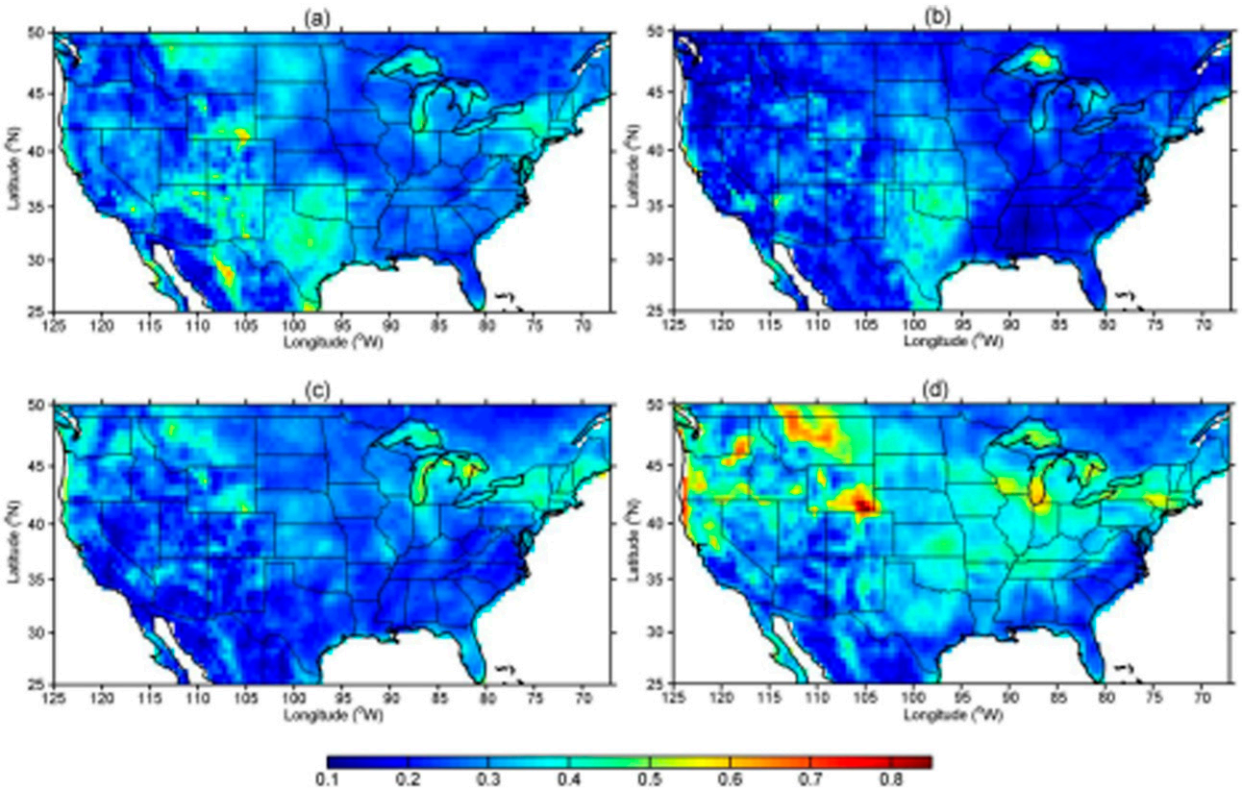

FIG. 3. As in Fig. 2, but for the interannual standard deviations of the 80-m wind speed ($m\,s^{-1}$).

areas covered by significant downward trends are considerably smaller compared to the other seasons.

A careful examination of the trend in the mean sea level pressure (MSLP) together with the 80-m wind vectors as shown in Fig. 5 helps explain the trend in the seasonal mean 80-m wind speed and its spatial distribution. In spring, a climatological anticyclonic cell over the eastern North Pacific Ocean results in a westerly 80-m wind over the western United States (Fig. 5a), which is further strengthened by a positive MSLP trend over the eastern North Pacific Ocean, leading to the region's upward trends in 80-m wind speed (Fig. 4a). The downward trends in wind speed along the Pacific coast (Fig. 4a) result from easterly winds induced by the trend in local anticyclonic cells (Fig. 5b). The springtime Bermuda high induces southeasterly and southerly winds into northeastern Mexico and the southern United States (Fig. 5a). The positive MSLP anomalies over the Gulf of Mexico (Fig. 5b) also strengthen the southerly winds, yielding an upward trend in the wind speed (Fig. 4a). The downward (upward) trends in 80-m wind speed over the Great Lakes region, the northeastern United States, and southern Canada (Fig. 4a) correspond to a positive MSLP anomaly over the Great Lakes region (Fig. 5b), which induces westerly (easterly) winds in areas north (south) of the Great Lakes and a strengthening (weakening) of the climatological westerly winds over the regions. The climatological summertime 80-m wind vector field across the United States (Fig. 5c) is similar to that in spring (Fig. 5a). The negative MSLP anomalies over the central and western United States (Fig. 5d) help produce positive westerly wind anomalies and thus the region's upward trend in the 80-m wind speed (Fig. 4b). In contrast, the negative trends in MSLP over the eastern United States (Fig. 5d) lead to the downward trends in wind speed in the region (Fig. 4b).

In autumn and winter, an anticyclonic cell occurs over the southeastern United States (Figs. 5e,g). In autumn, upward trends in the 80-m wind speed over the Great Plains can be explained by the positive MSLP trend over central United States (Fig. 5f), while negative MSLP trends over the eastern United States result in downward trends in the 80-m wind speed over the Great Lakes region and the Northeast (Fig. 4c). In winter, the large difference in the MSLP trends between the Pacific Ocean and the continental United States (Fig. 5h) accounts for the upward trend in wind speed over the western United States and northern Mexico (Fig. 4d). The positive trend in MSLP west of the Great Lakes and

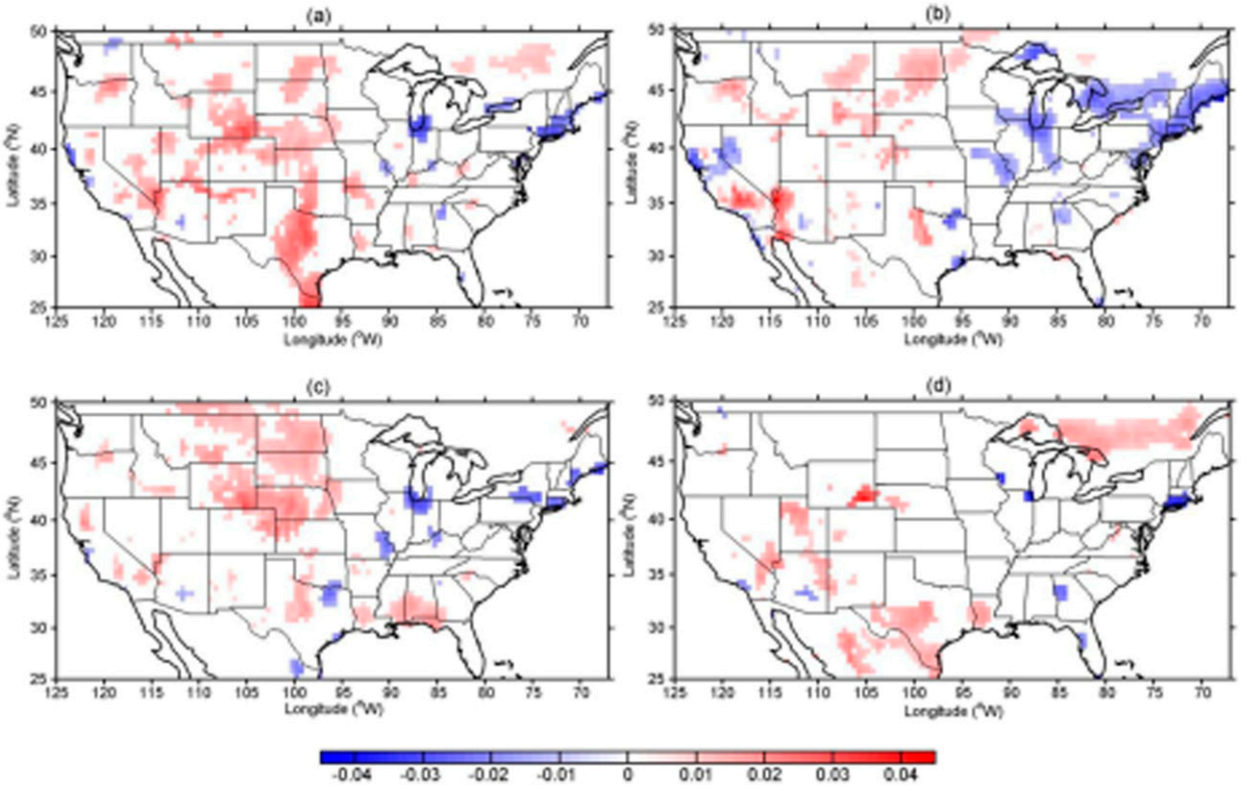

FIG. 4. As in Fig. 2, but for the linear trends in the 80-m wind speed ($m\,s^{-1}\,yr^{-1}$). The region at the 95% confidence level is shown.

the negative trend over the Great Lakes region and in the Northeast correspond to the downward wind speed trends in the northern states.

b. *Spatial and temporal patterns of the 80-m wind speed variability and the dominant climate forcing*

EOF analyses are performed to identify the prevailing spatial patterns of the interannual variability of the seasonal mean 80-m wind speed for the four seasons over the United States. Below, we discuss the results of the EOF analyses and the relationship between the leading EOF modes and the large-scale circulations.

1) THE FIRST MODE

The first EOF mode (Fig. 6) reveals that wind speed anomalies fluctuate in phase (same sign) across nearly entire United States in response to global climate anomalies. The total variance explained by the first mode varies from the lowest of 19.67% in summer, to the highest of 32.84% in winter. The time coefficients of the first mode are correlated significantly with the multivariate ENSO index (MEI; Wolter and Timlin 1993) and Niño-3.4 index significant at the 98% confidence level (Table 1) in spring, autumn, and winter. This provides evidence that ENSO is the primary climate forcing factor for the anomalies of seasonal mean 80-m wind speed during these seasons. The time coefficients of the first mode for summer are correlated with the summertime North Atlantic Oscillation (NAO) index, with a correlation coefficient of −0.46 significant at the 98% confidence level.

To understand the spatial patterns of the first EOF mode in the context of atmospheric circulation anomalies, the time series of the first EOF mode (PC1s) are regressed to the 200-hPa geopotential height (H200), the SST, the MSLP, and the 80-m wind vector. The results of the regression analyses are shown in Figs. 7 and 8.

A negative PNA pattern occurs in North America and North Pacific Ocean in spring, autumn, and winter (Wallace and Gutzler 1981) (Figs. 7a,e,g), as indicated by positive anomalous H200 centers over the North Pacific Ocean and much of the United States, and negative centers over the tropical eastern Pacific Ocean and Canada, although the position of the centers shift somewhat between seasons. The corresponding SST regression maps (Figs. 7b,f,h) show a La Niña pattern with positive (negative) SST anomalies over the tropical western Pacific and the central North Pacific (the central and eastern Pacific). Under the influence of a negative

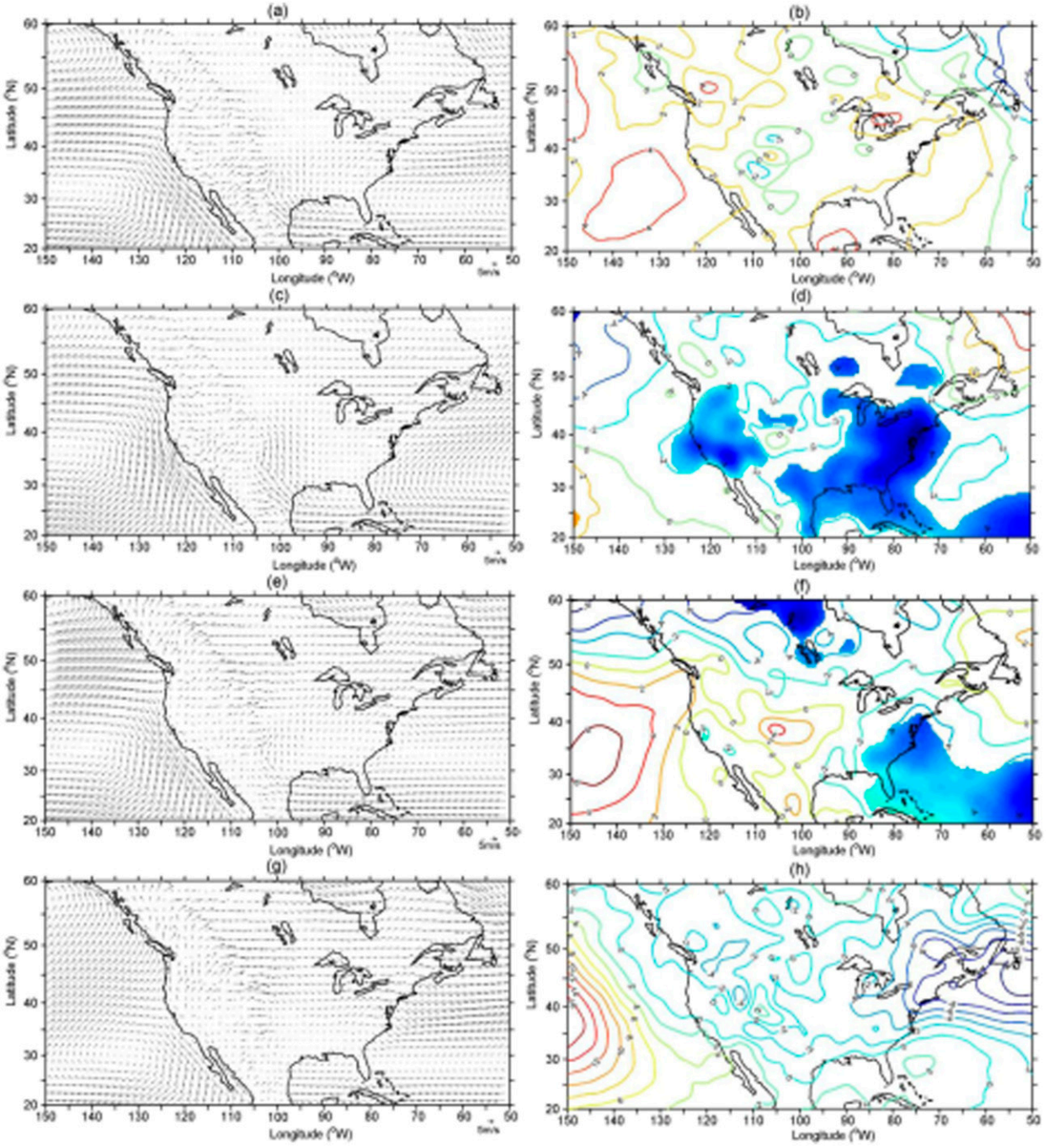

FIG. 5. Climatology of the (left) 80-m wind vectors and (right) trends in the mean sea level pressure (Pa yr^{-1}) in (a),(b) spring, (c),(d) summer, (e),(f) autumn, and (g),(h) winter. The filled regions are significant at the 95% confidence level.

PNA pattern induced by La Niña, the regression maps of MSLP (Figs. 8a,e,g) show positive (negative) anomalies over the eastern North Pacific and western North Atlantic (most of the North American continent). The anomalous 80-m westerly and northwesterly winds induced by the anomalous anticyclone over the eastern Pacific Ocean prevail over the western United States in spring, autumn, and winter, whereas the anomalous 80-m southerly and southwesterly winds induced by the anomalous anticyclone over the western North Atlantic dominate the central and eastern United States. The regression maps of 80-m wind field are similar to the

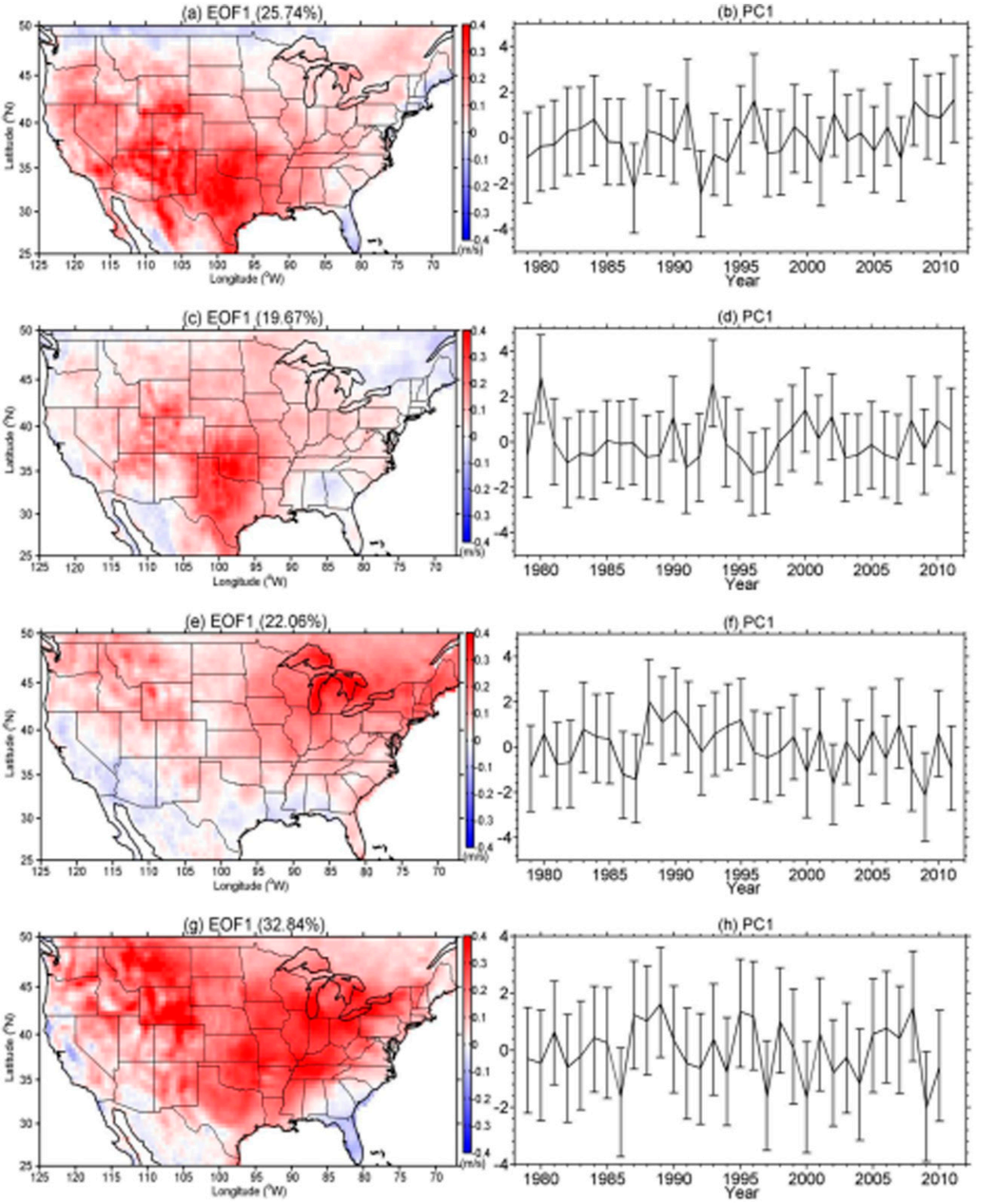

FIG. 6. (left) Spatial patterns and (right) the time series of the coefficients of the first EOF modes of the 80-m wind speed for the 1979–2011 period for (a),(b) spring, (c),(d) summer, (e),(f) autumn, and (g),(h) winter. The error bars of the 2.5% and 97.5% quantiles are added on the time series of the coefficients.

TABLE 1. Correlations between time coefficients of the first EOF modes and the multivariate ENSO index (MEI), Niño-3.4 index, the North Atlantic Oscillation (NAO) index, and El Niño Modoki index in spring, summer, autumn, and winter. Single and double asterisks indicate 99% and 98%, confidence levels, respectively.

Season	Spring	Summer	Autumn	Winter
MEI	−0.49*	−0.12	−0.40**	−0.48*
Niño-3.4	−0.47*	−0.15	−0.49*	−0.52*
NAO	−0.30	−0.46*	−0.02	0.21
El Niño Modoki	−0.20	0.03	−0.15	−0.23

maps of the climatological mean, which indicates that the negative phase of the PNA corresponds to a positive anomalous 80-m wind field and strengthens the 80-m wind speed across much of the United States; in contrast, the positive phase of the PNA weakens the 80-m wind speed.

In some regions of the United States, the nearly opposite directions between regressed and climatological 80-m winds result in negative 80-m wind speed anomalies of the first modes (Fig. 8). In spring (Fig. 8b), the regressed easterly winds near the U.S.–Canadian border west of the Great Lakes weakens the climatological westerly wind and results in the negative 80-m wind speed of the springtime first mode in this region (Fig. 6a). In autumn (Fig. 8f), the regressed southerly and southeasterly winds over the southwestern United States and northwestern Mexico offset the climatological northerly and northwesterly winds, yielding negative 80-m wind speed anomalies in these regions (Fig. 6e). In winter (Fig. 8h), the anomalous southerly wind induced by the anomalous anticyclone over the western North Atlantic Ocean weakens the climatological northerly wind and leads to negative 80-m wind speed anomalies over Florida (Fig. 6g).

Our findings are consistent with the results from several recent studies that examined the impacts of ENSO on wind resources in the Great Lakes region (Li et al. 2010) and the northern plains (Harper et al. 2007), and on wind gusts across most of the United States (Enloe et al. 2004). These studies also found a general increase of mean wind speeds and peak wind gusts during the cold phase of ENSO. However, Berg et al. (2013) found a general decrease of regional-averaged wintertime mean wind speeds over Southern California during La Niña, which is consistent with the negative 80-m wind speed anomaly over Southern California in Fig. 6g, although our results are based on reanalysis data whereas Berg et al. based their results on numerical simulations using the MM5 model.

In summer, a wave train occurs over the North Pacific Ocean, North America, and the North Atlantic Ocean (Fig. 7c) as indicated by positive H200 height anomalies over the western and eastern North Pacific Ocean, southeastern United States, eastern North Atlantic Ocean, and Greenland, and negative anomalies over the central North Pacific Ocean, northwestern United States, and the western North Atlantic Ocean. A similar wave train also occurs in the MSLP regression map (Fig. 8c). Negative (positive) H200 and MSLP anomalies over the western North Atlantic Ocean and western Europe (Greenland) represents a negative-phase NAO pattern. The correlation coefficient between the EOF time series and the NAO index in summer is −0.46, significant at the 98% confidence level. The regression (Fig. 8d) and the climatology (Fig. 5c) of the 80-m winds are similar over much of the United States, resulting in positive wind anomalies (Fig. 6c), but they are nearly opposite over the southeastern United States and Canada and western Mexico, yielding negative anomalies in these regions.

2) THE SECOND MODE

The total variance explained by the second EOF mode is approximately 15% with small variations between seasons. Unlike the first mode that explains the in-phase (same sign) fluctuation in response to climate forcing, the second mode captures the seesaw pattern (opposite sign or out of phase) between the northern and southern United States in spring (Fig. 9a), the eastern and western United States in summer and autumn (Figs. 9b,c), and the northeastern and southwestern United States in winter (Fig. 9d). Unlike the time series of the first mode that showed essentially no trend, the time series of the second mode in summer (Fig. 9d) displays an increasing trend. Moreover the spatial pattern of the second mode (Fig. 9c) in summer also resembles the spatial pattern of the 80-m wind speed trend in summer (Fig. 4b). Together, these suggest that the second mode may have contributed to the observed trend in summer. The results of wavelet analyses (not shown) indicate that the time series of the second modes have a major period of 2–3 yr for all seasons.

Similar regression analyses are also applied to the second mode and the results are shown in Figs. 10 and 11. In spring, the H200 and SST patterns suggest a positive phase of the springtime AO (Thompson and Wallace 1998) as indicated by the positive H200 anomalies in midlatitudes sandwiched between negative anomalies in the northern latitudes and the tropical Pacific Ocean (Fig. 10a) and the negative SST anomalies over the western North Atlantic Ocean, the tropical eastern Pacific Ocean, and the west coast of North America along with positive anomalies in the central North Pacific Ocean (Fig. 10b). Corresponding to this H200 pattern is

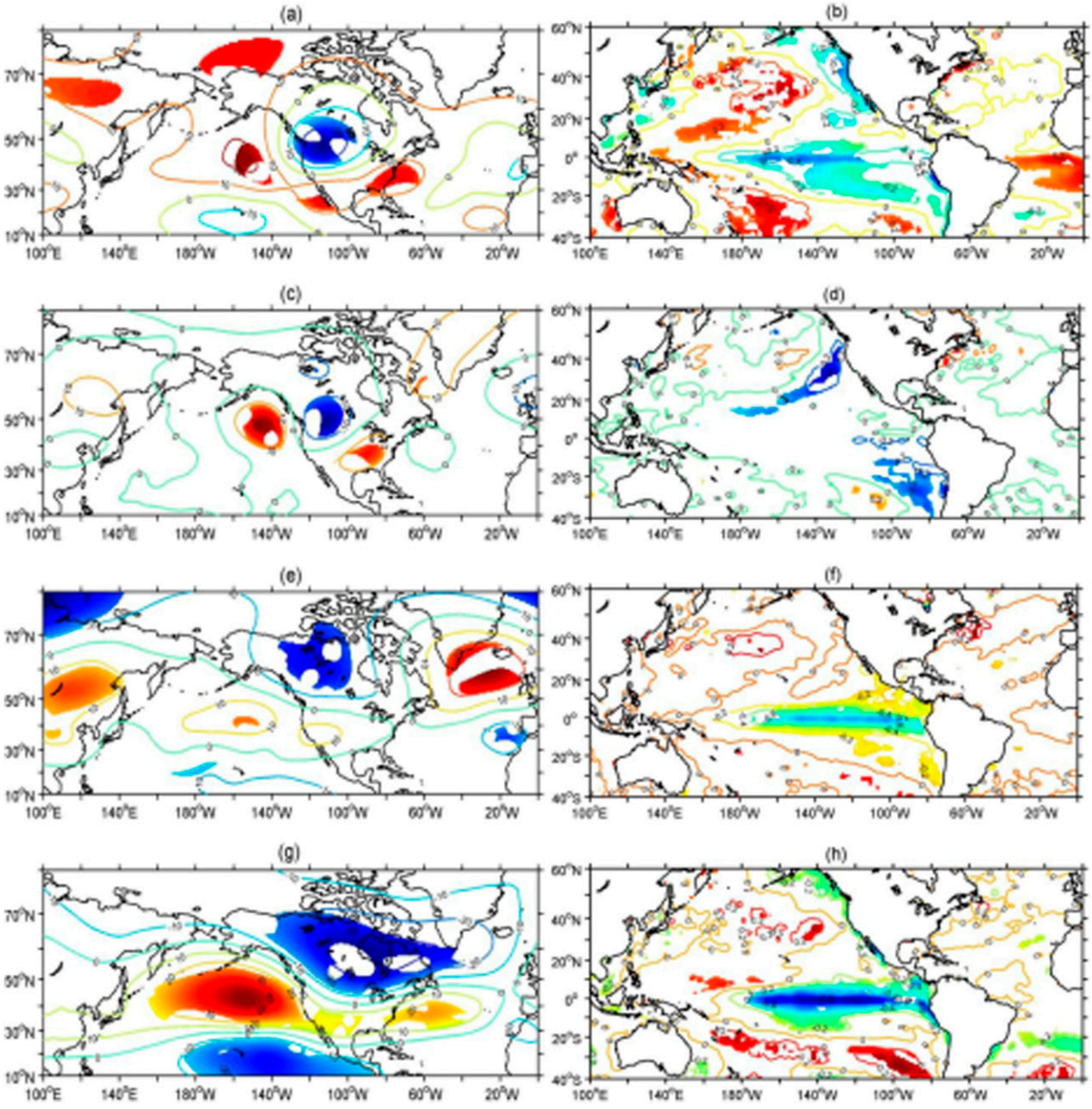

FIG. 7. (left) The anomalous 200-hPa geopotential height (gpm) and (right) sea surface temperature (SST; °C) maps regressed to the time series of the first EOF modes of 80-m wind speed for (a),(b) spring, (c),(d) summer, (e),(f) autumn, and (g),(h) winter for the period of 1979–2011. The filled regions are significant at the 95% confidence level.

an anomalous jet stream in the upper troposphere over the northern United States and southern Canada (not shown). Upper-level jet streams in this region, which are usually associated with cold air outbreaks and northerly low-level jets (Kapela et al. 1995), help to strengthen the 80-m wind speed north of 38°N (Fig. 10a). The large MSLP meridional gradients over the northern United States (Fig. 11a) also contribute to higher 80-m wind speed north of 38°N. The anomalous anticyclonic cell over the southeastern United States produces anomalous winds that are nearly opposite in direction to the springtime wind climatology south of 38°N, thus leading to negative 80-m wind speed anomalies of the second modes in this region (Fig. 11b).

In summer, a wave train occurs over the midlatitude study region with positive H200 centers over northern

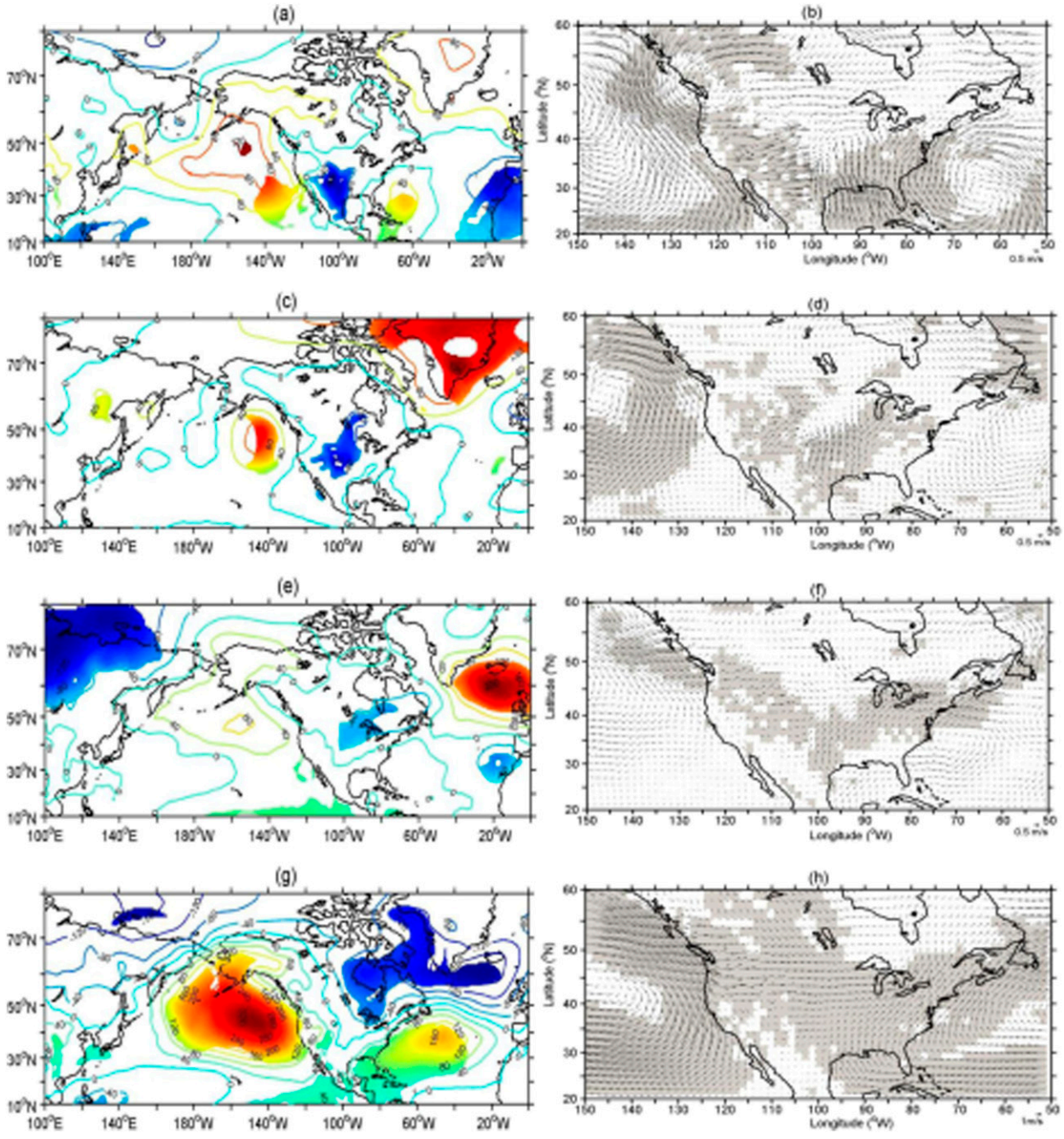

FIG. 8. As in Fig. 7, but for (left) the mean sea level pressure (Pa) and (right) 80-m wind vectors. The filled and shaded regions are significant at the 95% confidence level.

China, western Siberia, and northeastern North America and negative centers over Japan, northwestern North America, and the North Atlantic Ocean (Fig. 10c). This wave train bears some similarities with the circumglobal teleconnection (CGT) pattern (Ding and Wang 2005). Negative SST anomalies occur mainly over the tropical eastern Pacific Ocean, while positive SST anomalies are seen over the mid- to high-latitude regions of the North Pacific and Atlantic Oceans (Fig. 10d). An anomalous summertime upper troposphere jet stream associated with the H200 pattern is positioned over the northeastern Canada (not shown), which helps to strengthen (weaken) the 80-m wind speed in the central and western (eastern) United States. Near the surface, an anomalous cyclonic cell over the central United States (Fig. 11c) produces anomalous winds that are nearly opposite to the

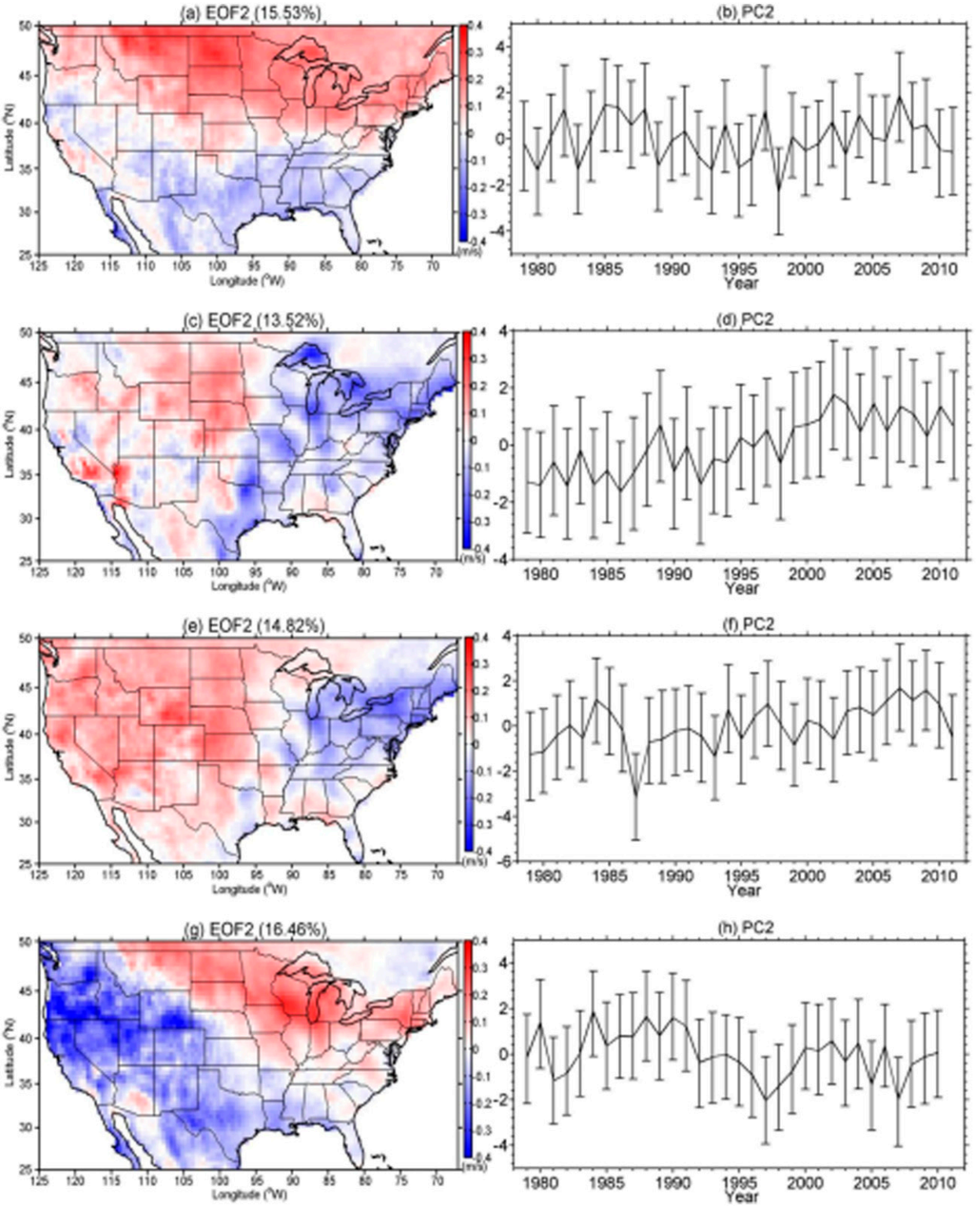

FIG. 9. As in Fig. 6, but for the second EOF modes.

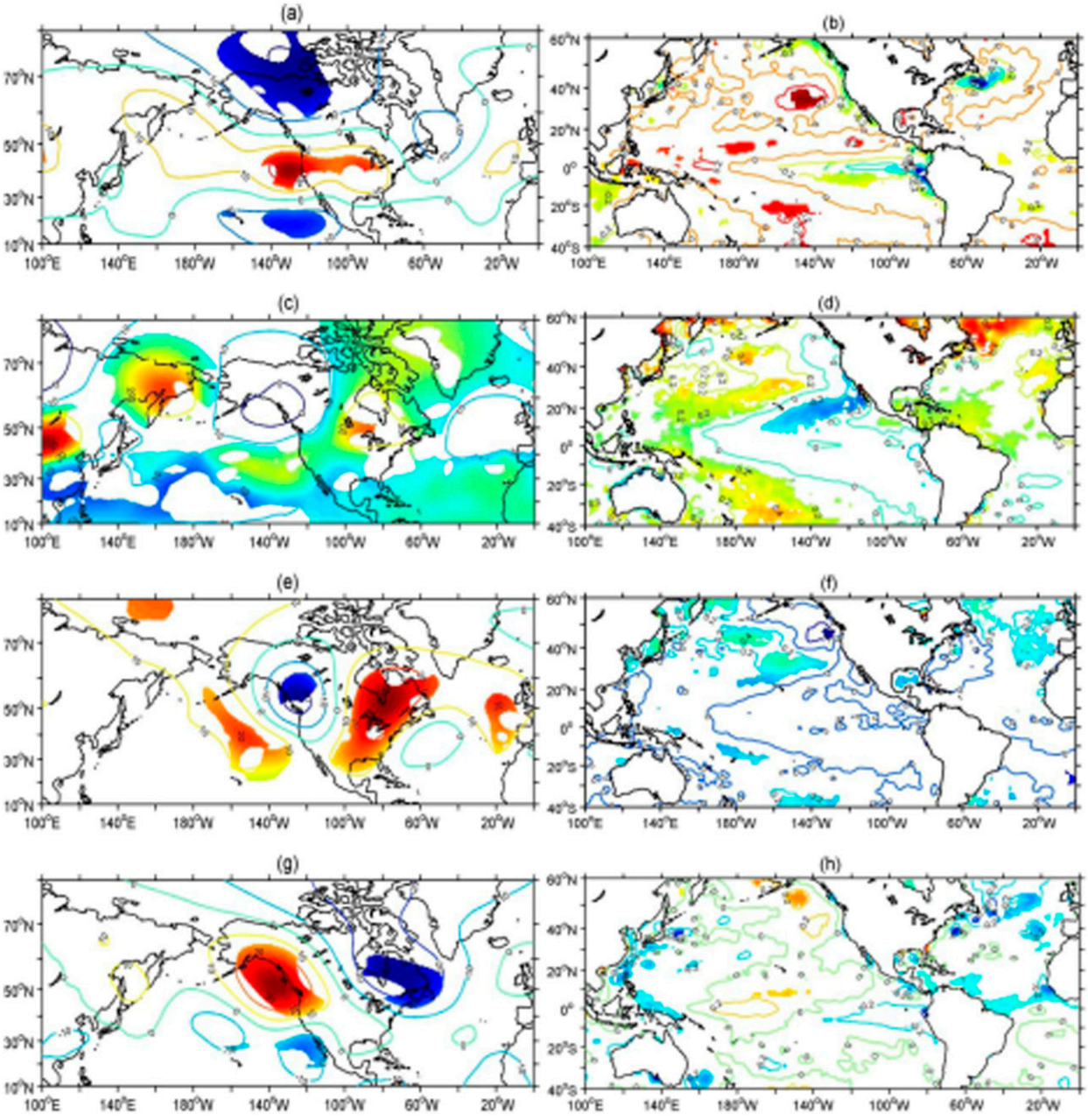

FIG. 10. As in Fig. 7, but for the second EOF modes.

summertime climatological winds, yielding a reduction in the 80-m wind speed. The anomalous easterly winds originating from the western Atlantic Ocean also weaken the climatological westerly winds over the Great Lakes region and areas of the Northeast.

In autumn, the anomalous SST pattern indicates a negative phase of the PDO (Mantua et al. 1997) (Fig. 10f). The correlation coefficient between the EOF time series and the time series of the PDO index in autumn is −0.38, significant at the 95% confidence level. A corresponding wave train occurs from western Pacific Ocean to North America and the North Atlantic Ocean (Fig. 10e), as indicated by positive H200 anomalies over the eastern North Pacific, eastern North America, and the eastern North Atlantic Ocean, and negative anomalies over the western North Atlantic Ocean and western North America. Corresponding to this H200 pattern is an anomalous jet stream over the western United States (not shown), which produces positive 80-m wind speed anomalies over the central and western United

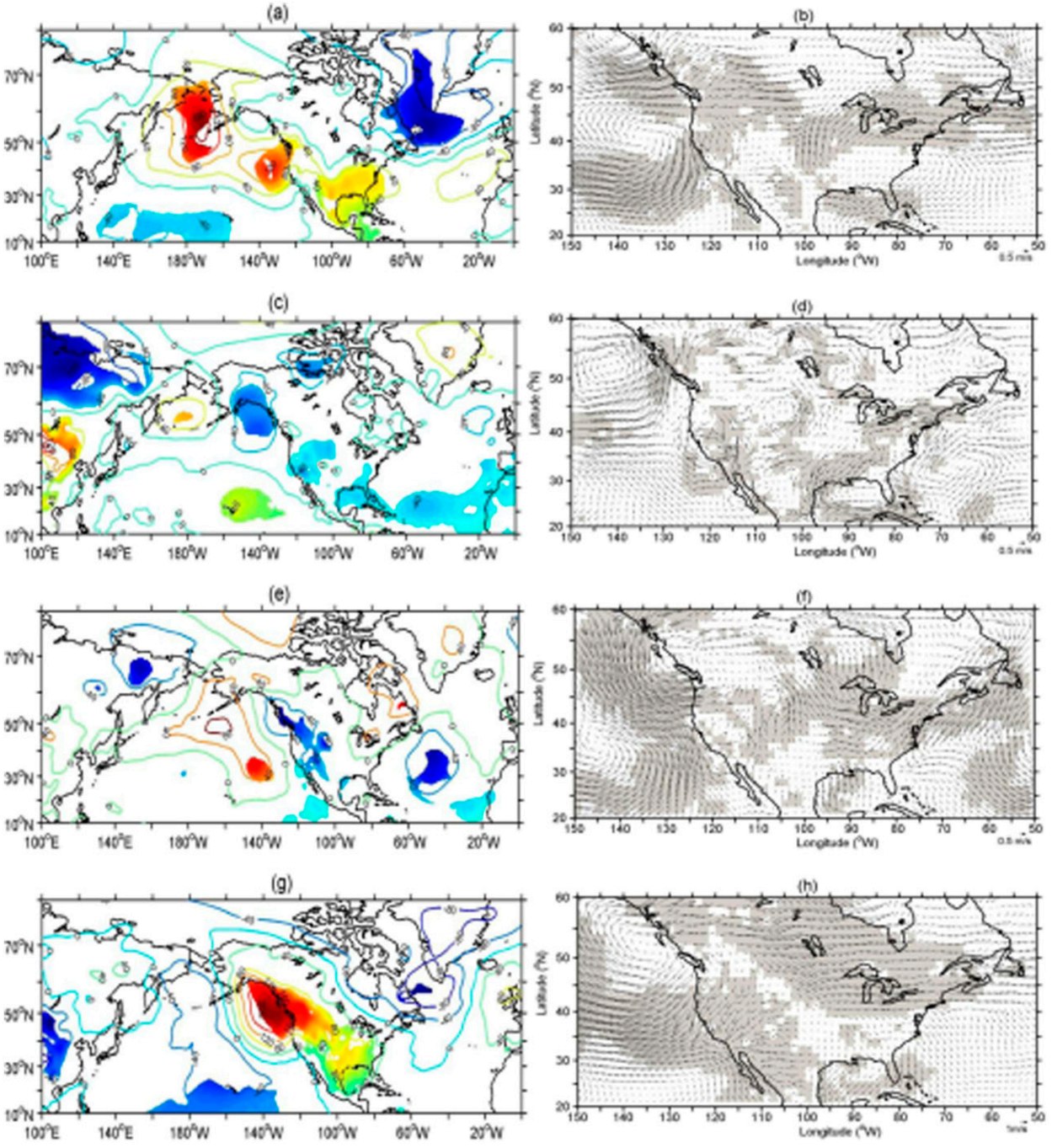

FIG. 11. As in Fig. 8, but for the second EOF modes.

States, but has little influence on winds over the eastern United States.

In winter, an anomalous jet stream (not shown) is active over the Great Lakes region and the northern Great Plains, resulting in positive wind speed anomalies in these regions. In contrast, a positive H200 anomaly over the western United States decreases the 80-m wind speed in the region. The anomalous SST pattern is similar to the El Niño Modoki pattern (Ashok et al. 2007). The correlation coefficient between the winter-time PC2 and the Modoki index is 0.36, significant at the 0.95% confidence level. The positive MSLP over western North America and the eastern North Pacific Ocean and the negative MSLP over northeastern North

America lead to anomalous 80-m easterly winds over much of the western United States and northwesterly and northerly winds over much of the northern Great Plains and the upper Midwest. These anomalous flows, when superimposed on the climatological wind patterns in these regions, explains the spatial patterns of the second mode for the season.

4. Summary

In this study, the spatial and temporal variability of the seasonal mean 80-m wind speeds over the contiguous United States for the 33-yr period from 1979 through 2011 are investigated using data from CFSR, a third-generation reanalysis dataset.

The climatology of the 80-m wind speed exhibits a strong seasonality, with stronger winds in the winter and weaker winds in the summer. In all seasons, the mean winds are generally stronger over the Midwest, the Great Plains, and the U.S. Northeast than over other regions of the country, especially the Intermountain West of the United States. The strongest winds are found over the Great Lakes, likely due to weaker friction over the lake surfaces. There is a detectable, but spatially variable, trend in the 80-m seasonal mean wind speed during the 33-yr period. Positive trends occur in areas of the Great Plains, the Intermountain West, and along parts of the Gulf coast from Louisiana through Alabama, while negative trends occur over areas of the Midwest, the Northeast, the U.S. Southeast, and areas of the Pacific coast.

The leading EOF modes reveal the prevailing spatial and temporal patterns in the wind speed variability. The first EOF mode, which shows in-phase variability across much of the United States, accounts for 25.74%, 19.67%, 22.06%, and 32.84% of the total variance in the 80-m wind speed, respectively, for spring, summer, autumn, and winter. The second mode accounts for 15.53%, 13.52%, 14.82%, and 16.46% of the total variance for the four seasons, respectively, and shows an out-of-phase variability primarily between north and south for spring, east and west for summer and autumn, and northeast and southwest for winter.

The regression analyses show that the first EOF mode is connected mainly to NAO in summer and to ENSO in other seasons. In all seasons except for summer, the anomalous H200 and MSLP patterns representing a negative-phase PNA pattern induced by La Niña produces a spatial pattern of wind anomalies that is similar to the climatological wind pattern, resulting in an increase in the 80-m wind speeds across much of the United States. In summer, the 80-m winds are also increased over much of the United States when the pattern of wind anomalies in response to the negative-phase NAO is, once again, similar to the climatological wind pattern.

The second modes for the four seasons are mainly related, respectively, to the spring AO, the summer CGT, the autumn PDO, and the winter El Niño Modoki. The anomalous upper-level jet stream associated with the H200 anomalies together with the MSLP anomalies help explain the seesaw pattern in the 80-m wind speed anomalies across the United States. In addition, the second modes may have contributed partially to the trends found for autumn, winter, and especially summer.

The above explanations for the two leading EOF modes are based on statistical considerations only. Numerical experiments are needed to further validate the forcing of SST anomalies over the North Pacific Ocean on the previously mentioned Rossby wave train. Nevertheless, the statistical relation can be very useful for developing seasonal predictions for 80-m wind speed and wind energy in the United States.

As a third-generation reanalysis product, the CFSR represents a substantial improvement over previous global reanalysis datasets. However, it also has limitations with implications for the interpretation of the results from the current study. First, as a global dataset, the horizontal resolution of the CFSR (0.5° latitude × 0.5° longitude) is still relatively low. The 0.5° grid spacing can smooth out spatial variability in the wind fields at scales less than about 50 km and underestimate the effect of local topographical gradients and land-use and land-cover changes on winds. Second, small biases of ocean wind stress from the CFSR dataset (Xue et al. 2011) may influence surface wind speeds across the United States, especially over the western and southeastern United States. Finally, the CFSR dataset has failed to reproduce the observed decreasing trend of surface wind speeds in some regions of the United States. These limitations, however, are unlikely to affect the confidence in the results of the current analyses.

Despite the limitations, the results about the dominant spatial and temporal patterns of the 80-m wind variability and the response to global climate anomalies may prove useful to the wind energy industry and energy policy makers. Although wind energy production is a function of wind variability on an hourly instead of seasonal time scale, climatological seasonal mean wind provides total wind energy potential in a given season. Understanding seasonal mean wind, its interannual variability, and the connection to large-scale circulation patterns can help identify a shift of seasonal wind energy relative to the climatology in a given year and thus improve seasonal forecasting of wind resources.

Acknowledgments. The authors thank the efforts made by NCEP in producing CFSR data. This research

is supported by the USDA Forest Service Northern Research Station under Research Joint Venture Agreement 11-JV-11242306-065 and by AgBioResearch of Michigan State University.

REFERENCES

American Wind Energy Association, 2013: AWEA U.S. wind industry annual market report. 130 pp. [Available online at http://www.awea.org/marketreports.]

Archer, C. L., and M. Z. Jacobson, 2003: Spatial and temporal distributions of U.S. winds and windpower at 80 m derived from measurements. *J. Geophys. Res.,* **108,** 4289, doi:10.1029/2002JD002076.

Ashok, K., S. K. Behera, S. A. Rao, H. Weng, and T. Yamagata, 2007: El Niño Modoki and its possible teleconnection. *J. Geophys. Res.,* **112,** C11007, doi:10.1029/2006JC003798.

Bao, X., and F. Zhang, 2013: Evaluation of NCEP–CFSR, NCEP–NCAR, ERA-Interim, and ERA-40 reanalysis datasets against independent sounding observations over the Tibetan Plateau. *J. Climate,* **26,** 206–214, doi:10.1175/JCLI-D-12-00056.1.

Benjamini, Y., and Y. Hochberg, 1995: Controlling the false discovery rate: A practical and powerful approach to multiple testing. *J. Roy. Stat. Soc.,* **57B,** 289–300.

Berg, N., A. Hall, S. B. Capps, and M. Hughes, 2013: El Niño–Southern Oscillation impacts on winter winds over Southern California. *Climate Dyn.,* **40,** 109–121, doi:10.1007/s00382-012-1461-6.

Breslow, P. B., and D. J. Sailor, 2002: Vulnerability of wind power resources to climate change in the continental United States. *Renewable Energy,* **27,** 585–598, doi:10.1016/S0960-1481(01)00110-0.

Chelliah, M., W. Ebisuzaki, S. Weaver, and A. Kumar, 2011: Evaluating the tropospheric variability in National Centers for Environmental Prediction's Climate Forecast System Reanalysis. *J. Geophys. Res.,* **116,** D17107, doi:10.1029/2011JD015707.

Chen, G., T. Iwasaki, H. Qin, and W. Sha, 2014: Evaluation of the warm-season diurnal variability over East Asia in recent reanalyses JRA-55, ERA-Interim, NCEP CFSR, and NASA MERRA. *J. Climate,* **27,** 5517–5537, doi:10.1175/JCLI-D-14-00005.1.

Clifton, A., and J. K. Lundquist, 2012: Data clustering reveals climate impacts on local wind phenomena. *J. Appl. Meteor. Climatol.,* **51,** 1547–1557, doi:10.1175/JAMC-D-11-0227.1.

Davis, R. E., B. P. Hayden, D. A. Gay, W. L. Phillips, and G. V. Jones, 1997: The North Atlantic subtropical anticyclone. *J. Climate,* **10,** 728–744, doi:10.1175/1520-0442(1997)010<0728:TNASA>2.0.CO;2.

Dee, D. P., and Coauthors, 2011: The ERA-Interim reanalysis: Configuration and performance of the data assimilation system. *Quart. J. Roy. Meteor. Soc.,* **137,** 553–597, doi:10.1002/qj.828.

DeGaetano, A. T., 1998: Identification and implications of biases in U.S. surface wind observation, archival, and summarization methods. *Theor. Appl. Climatol.,* **60,** 151–162, doi:10.1007/s007040050040.

Ding, Q., and B. Wang, 2005: Circumglobal teleconnection in the Northern Hemisphere summer. *J. Climate,* **18,** 3483–3505, doi:10.1175/JCLI3473.1.

Dvorak, M. J., E. D. Stoutenburg, C. L. Archer, W. Kempton, and M. Z. Jacobson, 2012: Where is the ideal location for a US East Coast offshore grid? *Geophys. Res. Lett.,* **39,** L06804, doi:10.1029/2011GL050659.

Elliott, D. L., C. G. Holladay, W. R. Barchet, H. P. Foote, and W. F. Sandusky, 1986: Wind energy resource atlas of the United States. U.S. Department of Energy Rep. DOE/CH10093-4, 210 pp.

Enloe, J., J. J. O'Brien, and S. R. Smith, 2004: ENSO impacts on peak wind gusts in the United States. *J. Climate,* **17,** 1728–1737, doi:10.1175/1520-0442(2004)017<1728:EIOPWG>2.0.CO;2.

Harper, B. R., R. W. Katz, and R. C. Harriss, 2007: Statistical methods for quantifying the effect of the El Niño–Southern Oscillation on wind power in the northern Great Plains of the United States. *Wind Eng.,* **31,** 123–137, doi:10.1260/030952407781998792.

Hua, G., X. Ming, and H. Qi, 2010: Changes in near-surface wind speed in China: 1969–2005. *Int. J. Climatol.,* **31,** 349–358.

Kapela, A. F., P. W. Leftwich, and R. Van Ess, 1995: Forecasting the impacts of strong wintertime post-cold front winds in the northern plains. *Wea. Forecasting,* **10,** 229–244, doi:10.1175/1520-0434(1995)010<0229:FTIOSW>2.0.CO;2.

Kempton, W., F. Pimenta, D. E. Veron, and B. A. Colle, 2010: Electric power from offshore wind via synoptic-scale interconnection. *Proc. Natl. Acad. Sci. USA,* **107,** 7240–7245, doi:10.1073/pnas.0909075107.

Klink, K., 1999a: Climatological mean and interannual variance of United States surface wind speed, direction and velocity. *Int. J. Climatol.,* **19,** 471–488, doi:10.1002/(SICI)1097-0088(199904)19:5<471::AID-JOC367>3.0.CO;2-X.

——, 1999b: Trends in mean monthly maximum and minimum surface wind speeds in the conterminous United States, 1961 to 1990. *Climate Res.,* **13,** 193–205, doi:10.3354/cr013193.

——, 2002: Trends and interannual variability of wind speed distributions in Minnesota. *J. Climate,* **15,** 3311–3317, doi:10.1175/1520-0442(2002)015<3311:TAIVOW>2.0.CO;2.

——, 2007: Atmospheric circulation effects on wind speed variability at turbine height. *J. Appl. Meteor. Climatol.,* **46,** 445–456, doi:10.1175/JAM2466.1.

Li, X., S. Zhong, X. Bian, and W. E. Heilman, 2010: Climate and climate variability of the wind power resources in the Great Lakes region of the United States. *J. Geophys. Res.,* **115,** D18107, doi:10.1029/2009JD013415.

Liléo, S., and O. Petrik, 2011: Investigation on the use of NCEP/NCAR, MERRA and NCEP/CFSR reanalysis data in wind resource analysis. *Proc. EWEA 2011 Conf.,* Brussels, Belgium, European Wind Energy Association. [Available online at http://www.ewea.org/annual2011/conference/conference-proceedings/.]

Long, C. S., A. H. Butler, S. Zhou, S. K. Yang, R. Lin, and J. Wild, 2011: Stratospheric characteristics of the NCEP climate forecast system reanalysis. *16th Conf. on the Middle Atmosphere,* Seattle, WA, Amer. Meteor. Soc., 522. [Available online at https://ams.confex.com/ams/91Annual/webprogram/Paper186058.html.]

Lu, J., G. A. Vecchi, and T. Reichler, 2007: Expansion of the Hadley cell under global warming. *Geophys. Res. Lett.,* **34,** L06805, doi:10.1029/2006GL028443.

Mantua, N. J., S. R. Here, Y. Zhang, J. M. Wallace, and R. C. Francis, 1997: A Pacific interdecadal climate oscillation with impacts on salmon production. *Bull. Amer. Meteor. Soc.,* **78,** 1069–1079, doi:10.1175/1520-0477(1997)078<1069:APICOW>2.0.CO;2.

McVicar, T. R., T. G. Van Niel, M. L. Roderick, L. T. Li, X. G. Mo, N. E. Zimmermann, and D. R. Schmatz, 2010: Observational evidence from two mountainous regions that near-surface wind speeds are declining more rapidly at higher elevations

than lower elevations: 1960–2006. *Geophys. Res. Lett.,* **37,** L06402, doi:10.1029/2009GL042255.

Nakicenovic, N., 2000: *Special Report on Emissions Scenarios.* Cambridge University Press, 612 pp.

Pryor, S. C., and J. Ledolter, 2010: Addendum to ''Wind speed trends over the contiguous United States.'' *J. Geophys. Res.,* **115,** D10103, doi:10.1029/2009JD013281.

——, and R. J. Barthelmie, 2011: Assessing climate change impacts on the near-term stability of the wind energy resource over the United States. *Proc. Natl. Acad. Sci. USA,* **108,** 8167–8171, doi:10.1073/pnas.1019388108.

——, and Coauthors, 2009: Wind speed trends over the contiguous United States. *J. Geophys. Res.,* **114,** D14105, doi:10.1029/2008JD011416.

Rahim, N. A. A., L. Juneng, and F. T. Tangang, 2013: Wind-wave simulation in South China Sea: Preliminary results of model evaluation using different wind forcing. *AIP Conf. Proc.,* **1571,** 454, doi:10.1063/1.4858697.

Rauthe, M., A. Hense, and H. Paeth, 2004: A model intercomparison study of climate change signals in extratropical circulation. *Int. J. Climatol.,* **24,** 643–662, doi:10.1002/joc.1025.

Saha, S., and Coauthors, 2006: The NCEP Climate Forecast System. *J. Climate,* **19,** 3483–3517, doi:10.1175/JCLI3812.1.

——, and Coauthors, 2010: The NCEP Climate Forecast System Reanalysis. *Bull. Amer. Meteor. Soc.,* **91,** 1015–1057, doi:10.1175/2010BAMS3001.1.

——, and Coauthors, 2014: The NCEP Climate Forecast System version 2. *J. Climate,* **27,** 2185–2208, doi:10.1175/JCLI-D-12-00823.1.

Sailor, D. J., M. Smith, and M. Hart, 2008: Climate change implications for wind power resources in the northwest United States. *Renewable Energy,* **33,** 2393–2406, doi:10.1016/j.renene.2008.01.007.

Segal, M., Z. Pan, R. W. Arritt, and E. S. Takle, 2001: On the potential change in wind power over the US due to increases of atmospheric greenhouse gases. *Renewable Energy,* **24,** 235–243, doi:10.1016/S0960-1481(00)00194-4.

Seidel, D. J., Q. Fu, W. J. Randel, and T. J. Reichler, 2008: Widening of the tropical belt in a changing climate. *Nat. Geosci.,* **1,** 21–24, doi:10.1038/ngeo.2007.38.

Smith, T. M., and R. W. Reynolds, 2003: Extended reconstruction of global sea surface temperature based on COADS data (1854–1997). *J. Climate,* **16,** 1495–1510, doi:10.1175/1520-0442-16.10.1495.

——, and ——, 2004: Improved extended reconstruction of SST (1854–1997). *J. Climate,* **17,** 2466–2477, doi:10.1175/1520-0442(2004)017<2466:IEROS>2.0.CO;2.

Smits, A., A. M. G. Klein-Tank, and G. P. Können, 2005: Trends in storminess over the Netherlands, 1962–2002. *Int. J. Climatol.,* **25,** 1331–1344, doi:10.1002/joc.1195.

St. George, S., and S. A. Wolfe, 2009: El Niño stills winter winds across the southern Canadian Prairies. *Geophys. Res. Lett.,* **36,** L23806, doi:10.1029/2009GL041282.

Thompson, D. W. J., and J. M. Wallace, 1998: The Arctic Oscillation signature in the wintertime geopotential height and temperature fields. *Geophys. Res. Lett.,* **25,** 1297–1300, doi:10.1029/98GL00950.

Vautard, R., J. Cattiaux, P. Yiou, J.-N. Thépaut, and P. Ciais, 2010: Northern Hemisphere atmospheric stilling partly attributed to an increase in surface roughness. *Nat. Geosci.,* **3,** 756–761, doi:10.1038/ngeo979.

Wallace, J. M., and D. Gutzler, 1981: Teleconnection in the geopotential height field during the Northern Hemisphere winter. *Mon. Wea. Rev.,* **109,** 784–812, doi:10.1175/1520-0493(1981)109<0784:TITGHF>2.0.CO;2.

Wan, H., X. L. Wang, and V. R. Swail, 2010: Homogenization and trend analysis of Canadian near-surface wind speeds. *J. Climate,* **23,** 1209–1225, doi:10.1175/2009JCLI3200.1.

Wang, W., P. Xie, S.-H. Yoo, Y. Xue, A. Kumar, and X. Wu, 2011: An assessment of the surface climate in the NCEP Climate Forecast System Reanalysis. *Climate Dyn.,* **37,** 1601–1620, doi:10.1007/s00382-010-0935-7.

Westrick, K. J., P. Storck, and T. Hiester, 2005: Improving the economics of wind through forecasting. *North Amer. Windpower,* **2,** 20–22.

Wilks, D. S., 2011: *Statistical Methods in the Atmospheric Sciences.* 3rd ed. Elsevier, 676 pp.

Wolter, K., and M. S. Timlin, 1993: Monitoring ENSO in COADS with a seasonally adjusted principal component index. *Proc. 17th Climate Diagnostics Workshop,* Norman, OK, NOAA/NMC/CAC, 52–57.

Xu, M., C.-P. Chang, C. Fu, Y. Qi, A. Robock, D. Robinson, and H. Zhang, 2006: Steady decline of East Asian monsoon winds, 1969–2000: Evidence from direct ground measurements of wind speed. *J. Geophys. Res.,* **111,** D24111, doi:10.1029/2006JD007337.

Xue, Y., B. Huang, Z.-Z. Hu, A. Kumar, C. Wen, D. Behringer, and S. Nadiga, 2011: An assessment of oceanic variability in the NCEP Climate Forecast System Reanalysis. *Climate Dyn.,* **37,** 2511–2539, doi:10.1007/s00382-010-0954-4.

Yuan, X., E. F. Wood, L. Luo, and M. Pan, 2011: A first look at Climate Forecast System version 2 (CFSv2) for hydrological seasonal prediction. *Geophys. Res. Lett.,* **38,** L13402, doi:10.1029/2011GL047792.